SI Appendix

Content
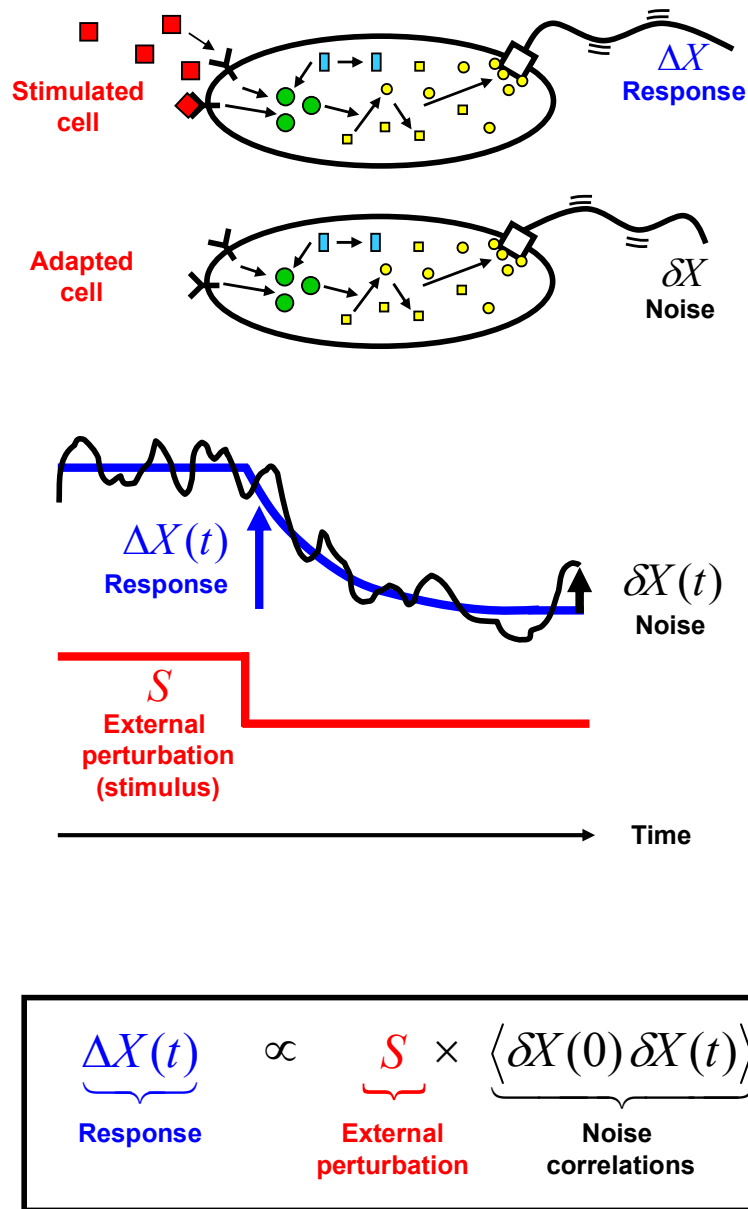
1. Inferring cellular response from noise measurements in bacterial chemotaxis

In this paper, we identify a general relationship between the fluctuations of cellular behavior in single cells and the cellular response to an external stimulus in bacterial chemotaxis.

Signal processing in cells is subject to fluctuations, or noise, arising not only from the external environment but also from the intracellular molecular reactions. A series of single-cell experiments has demonstrated that molecular noise can sometimes promote phenotype variability within an isogenic population of cells (1-6). The significance of molecular noise for phenotypic variability has been reported in a number of biological processes as diverse as gene expression and signal transduction in prokaryotes and eukaryotes (7, 8). A common factor between these noisy biological systems is that phenotypic variability emerges from the amplification of random molecular events by a sensitive intracellular mechanism (9, 10). It is therefore conceivable that the same biological systems that are sensitive to intracellular noise are also sensitive to small extra-cellular perturbations such as a sudden change in the environment.

It has been known since the early twentieth century that the study of temporal fluctuations in the output signal of a physical system can yield quantitative information about the underlying dynamics of the system. The explicit relationship between the noise in the output signal of a system that is in equilibrium with its environment and the response of that system to small external perturbations was depicted in a general mathematical expression called the fluctuation-dissipation relation (11-13).

Making use of the fluctuation-dissipation relation, we characterize the underlying principles governing the relationship between behavioral variability inherent in individual non-stimulated cells and the macroscopic cellular response in bacterial chemotaxis (Figure S1). In our previous experimental work (1) we focused solely on the characterization of the noise in chemotaxis for non-stimulated cells. The present model goes beyond this initial study by showing that one can predict the cellular response of stimulated cells in measuring the noise in non-stimulated cells.

Figure S1: Inferring cellular response from noise measurements in bacterial chemotaxis. The "fluctuation-dissipation relation" establishes that when a physical system is at equilibrium, the macroscopic response of the system to small external perturbations is related to the fluctuation properties of the system at equilibrium (11-13). In a biological system, the fluctuation-dissipation relation can be used to infer the response of a cell to a small external perturbation, the stimulus S (red), by measuring the fluctuations $\delta X(t)$ in the cellular behavior of adapted non-stimulated single cells (black). The macroscopic cellular response $\Delta X(t)$ (blue) is proportional to the product of the external perturbation and the autocorrelation of the spontaneous fluctuations.

2. Stochastic model of adaptation in bacterial chemotaxis

In the present section we develop a stochastic model of adaptation in bacterial chemotaxis. We model the chemotaxis pathway combining the two-state model of receptors originally proposed by Asakura and Honda (14) with the exact adaptation mechanism proposed by Barkai and Leibler (15). The phosphorylation cascade is similar to the one in Sourjik and Berg (16). The resulting kinetic model is essentially the same as the kinetic models used by Morton-Firth et al. (17), Melo and Tu (18), Rao et al. (19) and Kollman et al. (20). We provide parameter values for our model in Table S1. We also list in Table S2 the parameter values from previously published models (17, 19, 20).

2.1 Kinetic model.

Ligand binding and conformational changes are much faster than the (de)methylations reactions and therefore operate at quasi-equilibrium on the time scales relevant for the adaptation process. Under these conditions we describe the activity of receptor complexes using equilibrium probabilities a_m (15, 18, 19, 21) (Figures 1B and S7). This probability depends on the level of methylation of the receptor complexes that ranges within $m = 0, \ldots, m_{\max}$, where $m_{\max}$ is the maximal number of methylation sites. The probability a_m is a function of the ligand concentration, L, present in the external medium. We assume that receptor complexes with zero methyl groups are always inactive while receptor complexes with $m_{\max}$ methyl groups are always active: $a_0 = 0$ and $a_{m_{\max}} \cong 1$. For non-saturating amount of attractants (sub-milimolar concentrations of aspartate) these boundary conditions are supported by experimental results (16) and ensure exact adaptation (18). At larger stimuli (e.g. concentrations of α-methyl-DL-aspartate larger than 10 mM) $a_{m_{\max}}$ decreases below one with increasing amount of ligand (16, 20). A complex cooperative mechanism between receptors governs the sensitivity of the chemotaxis receptors to changes in ligand concentration (21-28). To keep our analysis both general and independent of a specific model of receptors, we will use the probability a_m directly as the input signal to the adaptation module without specifying dependency of a_m on the ligand concentration L. However, for the stochastic numerical simulations presented in this paper, we specify the relationship between a_m and L using stochastic models of receptors (17) (see SI Sec. 7).

We make a distinction between the concentration of free receptor complexes X_m and the concentrations of the intermediate compounds, the receptor-CheR X_{rm} and receptor-CheBp X_{bm}. The subscript m indicates the methylation level of the receptor-complex. The total concentration of free active and inactive receptor-kinase complexes are then $A^* = \sum_m a_m X_m$ and $A = \sum_m (1 - a_m) X_m$, respectively. We model methylation and demethylation of the receptors assuming Michaelis-Menten kinetics for the individual methylation-demethylation steps. To ensure exact adaptation of the system we use the mechanism proposed by Barkai and Leibler (15) and extended by Morton-Firth et al. (17), Mello and Tu (18)and Rao et al. (19): CheR binds only inactive receptor

complexes, whereas CheB-P binds only active complexes. For comparison, in SI Sec. 6 we consider the case where CheR binds receptor complexes irrespective of their activity state. The velocity of methylation of receptors with m methyl groups is $r(1-a_m)X_m$ and the velocity of demethylation is $ba_m X_m$, where the rates of methylation, $r = k_r \varepsilon_r /(K_r + A)$, and demethylation, $b = k_b \varepsilon_{bp} /(K_b + A^*)$, are defined in Equation (1). Here ε_r and ε_{bp} are the total concentrations of CheR and CheB-P, K_r and K_b are effective Michaelis-Menten constants, and k_r, k_b are the corresponding catalytic rates. From the Michaelis-Menten approximation we obtain the concentrations of the intermediate compounds as function of the concentration of the free receptor complexes:

$$X_{rm} = \frac{r}{k_r}(1-a_m)X_m \tag{S1}$$

$$X_{bm} = \frac{b}{k_b}a_m X_m \tag{S2}$$

Summing up X_m, X_{rm} and X_{bm} for all m we obtain the mass conservation equation (2):

$$A\left(1+\frac{r}{k_r}\right) + A^*\left(1+\frac{b}{k_b}\right) = 1 \tag{S3}$$

We normalize the concentrations with the total concentration of receptor complexes in the system: X_m, A, A^*, ε_r, ε_{bp}, K_r and K_b are expressed as fractions of the total number, N, of receptor complexes in the system. The total kinase activity of the system, A_{tot}^*, includes the activity of the free receptor complexes as well as the activity of the receptor-CheB-P compounds

$$A_{tot}^* = A^*\left(1+\frac{b}{k_b}\right) \tag{S4}$$

The time evolution of the concentrations of receptor complexes with $m = 0,\ldots,m_{\max}$ methyl groups (Figure 2B) is governed by the following kinetic equation (eq. (5) in the main text):

$$\frac{d}{dt}X_m = r\left[(1-a_{m-1})X_{m-1} - (1-a_m)X_m\right] + b\left[a_{m+1}X_{m+1} - a_m X_m\right] \tag{S5}$$

5

The rates r and b are defined in Eq. (1). Multiplying Eq. (S5) with m and summing over all m's yields Eq. (1). We model the phosphorylation cascade using mechanisms and parameter values similar to those proposed by Sourjik and Berg (29) and used subsequently by Rao et al. (19) and Kollman et al. (20):

$$\frac{d}{dt}\varepsilon_{bp} = a_b A_p \left(\varepsilon_b - \varepsilon_{bp}\right) - d_b \frac{K_b}{K_b + A^*}\varepsilon_{bp} \tag{S6}$$

$$\frac{d}{dt}Y_p = a_y A_p (\varepsilon_y - Y_p) - d_y Y_p \tag{S7}$$

$$\frac{d}{dt}A_p = k_p A_{tot}^* (1 - A_p) - a_y A_p (\varepsilon_y - Y_p) - a_b A_p \left(\varepsilon_b - \varepsilon_{bp}\right) \tag{S8}$$

ε_b and ε_y are the total concentrations of CheB and CheY, respectively which remain constant. The total concentration of CheB-P, ε_{bp}, includes the concentration of free molecules of CheB-P, B_p, plus the concentration of receptors bound to CheB-P: $\sum_m X_{bm} = A^* \varepsilon_{bp} /(K_b + A^*)$. Thus, we can express the concentrations of free molecules of CheB and CheB-P as function of ε_{bp}:

$$B = \varepsilon_b - \varepsilon_{bp} \tag{S9}$$

$$B_p = \frac{K_b}{K_b + A^*}\varepsilon_{bp} \tag{S10}$$

Inserting equations (S9) and (S10) in the kinetic equation describing the negative feedback via phosphorylation of CheB, $dB/dt = d_b B_p - a_b A_p B$, yields equation (S6). Similarly, equation (S7) describes the phosphorylation and de-phosphorylation of CheY. Phosphate transferase to CheB and CheY are simplified into bimolecular reactions with rates a_b and a_y, respectively (19, 20, 29). De-phosphorylation rates are d_b and d_y, respectively, with the latter including the effect of the phosphatase CheZ. A_p is the concentration of phosphorylated kinases. k_p is the autophosphorylation rate of active kinases. Because a kinase must be active in order to bind a phosphate group, the autophosphorylation rate of the kinase is proportional to the probability for the kinase to be active, i.e. the normalized number of active kinases A_{tot}^* (19, 20, 29).

2.2 Steady state analysis

At steady state, equations (S7) and (S8) yield the steady state concentrations of CheY-P ($\overline{Y}_p$) and CheA-P ($\overline{A}_p$) as function of $\overline{A}$, $\overline{A}^*$ and $\overline{\varepsilon}_{bp}$:

$$\overline{A}_p = \left[1 + \frac{a_y(\varepsilon_y - \overline{Y}_p) + a_b(\varepsilon_b - \overline{\varepsilon}_{bp})}{k_p A_{tot}^*}\right]^{-1} \tag{S11}$$

$$\overline{Y}_p = \varepsilon_y + \frac{a_y}{2}\left(\frac{k_p \overline{A}_{tot}^*}{d_y a_y} - \frac{\varepsilon_y}{a_y}\right) + \frac{d_y}{2}\left(\frac{k_p \overline{A}_{tot}^*}{d_y a_y} + \frac{a_b(\varepsilon_b - \overline{\varepsilon}_{bp})}{d_y a_y}\right) -$$
$$\left\{\left[\frac{a_y}{2}\left(\frac{k_p \overline{A}_{tot}^*}{d_y a_y} - \frac{\varepsilon_y}{a_y}\right) + \frac{d_y}{2}\left(\frac{k_p \overline{A}_{tot}^*}{d_y a_y} + \frac{a_b(\varepsilon_b - \overline{\varepsilon}_{bp})}{d_y a_y}\right)\right]^2 + d_y \varepsilon_y\left(\frac{k_p \overline{A}_{tot}^*}{d_y a_y} + \frac{a_b(\varepsilon_b - \overline{\varepsilon}_{bp})}{d_y a_y}\right)\right\}^{1/2} \tag{S12}$$

Replacing $\overline{Y}_p$ and $\overline{A}_p$ in equation (S6) we obtain an algebraic relation between $\overline{A}$, $\overline{A}^*$ and $\overline{\varepsilon}_{bp}$. Equations (1) and (S3) provide the other two relations necessary to solve the system. Using equation (1) we can eliminate one of the unknown by expressing $\overline{A}^*$ as function of $\overline{A}$ and $\overline{\varepsilon}_{bp}$:

$$\overline{A}^* = \frac{\alpha K_b \overline{A}}{K_r + \overline{A} - \alpha \overline{A}} \tag{S13}$$

where α is the ratio of the maximum enzymatic velocities:

$$\alpha = \frac{k_r \varepsilon_r}{k_b \overline{\varepsilon}_{bp}} \tag{S14}$$

Thus, we are left with a system of two algebraic equations for the two unknown $\overline{A}$ and $\overline{\varepsilon}_{bp}$. The first relation is the feedback loop equation (S6), the second relation is the mass conservation equation (S3), which after substitution of equation (S13) becomes:

$$\overline{A}^3(1-\alpha) + \overline{A}^2\left[(K_r + \alpha K_b) + (1-\alpha)(\varepsilon_r + \alpha\overline{\varepsilon}_{bp} - 1 + K_r)\right]$$
$$+ \overline{A} K_r\left(K_r + \alpha K_b + \varepsilon_r + \alpha\overline{\varepsilon}_{bp} + \alpha - 2\right) - K_r^2 = 0 \tag{S15}$$

Equation (S15) is *identical* to the equation found by Goldbeter and Koshland for a covalent modification system (caption of Figure 3 on p. 6842 of (30)). We solve equation (S15) and (S6) with the NSolve[] routine of the software Mathematica 5.2 using the parameter values listed in Table S1. We obtain $\overline{A}$ and $\overline{\varepsilon}_{bp}$ for a range of CheR concentrations ε_r. The other variables, $\overline{A}^*$, $\overline{Y}$, $\overline{Y}_p$, $\overline{A}_p$, $\overline{r}$, $\overline{b}$, $\overline{B}$, $\overline{B}_p$ and the total kinase activity of the system $\overline{A}_{tot}^* = \overline{A}^*\left(1 + \overline{b}/k_b\right)$ follow easily from equations (1, S9–S13). When considering the system without the CheB-P feedback loop, we assume that ε_{bp} is

constant and equal to its wild type value at steady state and solve equation (S15) to obtain $\overline{A}$. Figures 2A and 2B show $\overline{A}_{tot}^{*}$ as function of ε_r calculated without and with the CheB-P feedback loop, respectively (parameter values are in Table S1).

Remarkably, the steady state of the total kinase activity and of the concentration of CheY-P are independent from the activation probabilities $a_m(L)$ and therefore of the amount of ligand in the external medium (Equations S6 and S15 are independent from $a_m(L)$). As a consequence the bacterial chemotaxis system exhibits exact adaptation at the population level. This result is a direct consequence of the assumption made earlier, that CheR only binds inactive receptors and CheB-P only binds active receptors (17-19). If instead we assume that CheR binds receptor complexes irrespective of their activity, then exact adaptation may be lost whenever the fraction of fully methylated receptors becomes important (18).

Although $\overline{A}_{tot}^{*}$ and $\overline{Y}_p$ are independent from the amount of ligand in the external medium, the distribution of receptors among methylation levels is not. From equation (S5) and (1) we obtain the steady state of X_m:

$$\overline{X}_m = \frac{h_m}{\sum\limits_{m=0}^{m_{\max}} h_m}\left(\overline{A} + \overline{A}^{*}\right) \quad \text{with} \quad h_m = \frac{(1-\overline{a}_0)(1-\overline{a}_1)...(1-\overline{a}_{m-1})}{\overline{a}_1\overline{a}_2\cdots\overline{a}_m}\left(\frac{\overline{A}^{*}}{\overline{A}}\right)^m \quad (S16)$$

and $h_0 = 1$. The steady states of the compounds $\overline{X}_{rm}$ and $\overline{X}_{rm}$ follow from equations (S1) and (S2).

In previous models of bacterial chemotaxis (17, 19, 20), the probability of activation of receptors complexes at steady state increases approximately linearly with the number of methyl groups, $\overline{a}_m \approx m/m_{\max}$, when the external concentration of ligand is small (Fig. S7). In this simple case we find that the steady state distribution of free receptors among methylation levels becomes approximately binomial

$$\frac{\overline{X}_m}{\overline{A}+\overline{A}^{*}} \cong \binom{m_{\max}}{m}\left(\frac{\overline{A}^{*}}{\overline{A}+\overline{A}^{*}}\right)^m\left(\frac{\overline{A}}{\overline{A}+\overline{A}^{*}}\right)^{m_{\max}-m} \quad (S17)$$

with mean $m_{\max}\overline{A}^{*}/(\overline{A}+\overline{A}^{*})$ and standard deviation $\sqrt{m_{\max}\overline{A}\,\overline{A}^{*}}/(\overline{A}+\overline{A}^{*})$ (see Figure S6A below).

2.3 Perturbation analysis of the kinetic system.

In this section we present a linear perturbation analysis of the chemotaxis system around the steady state, including the feedback loop in CheB-P. We consider only small perturbations of the dynamical variables of the system in response to a small sudden increase or decrease of ligand concentration in the external medium. Linearization of

equations (1) and (S3) around steady state yields the following equations for the time evolution of the linear perturbation of ΔM and ΔA as function of ΔA^* and $\Delta\varepsilon_{bp}$:

$$\frac{d}{dt}\Delta M = -\underbrace{\left(k_r\theta_r\frac{1+\theta_b}{1+\theta_r}+k_b\theta_b\right)}_{\tau_{GK}^{-1}}\Delta A^* - \underbrace{\left(1+\frac{k_r}{k_b}\frac{\theta_r}{1+\theta_r}\right)k_b\theta_c}_{g_b}\Delta\varepsilon_{bp} \tag{S18}$$

$$\Delta A = -\frac{1+\theta_b}{1+\theta_r}\Delta A^* - \frac{\theta_c}{1+\theta_r}\Delta\varepsilon_{bp} \tag{S19}$$

The factors θ_r and θ_b are the fractions of perturbed inactive and active receptors that are bound to CheR and CheB-P respectively, while θ_c represents the fraction of CheB-P molecules that are bound to active receptors:

$$\theta_r = \frac{K_r\varepsilon_r}{\left(K_r+\overline{A}\right)^2}\,, \qquad \theta_b = \frac{K_b\overline{\varepsilon}_{bp}}{\left(K_b+\overline{A}^*\right)^2}\,, \quad \text{and } \theta_c = \frac{\overline{A}^*}{K_b+\overline{A}^*} = \frac{\overline{b}\,\overline{A}^*}{k_b\overline{\varepsilon}_{bp}}\,. \tag{S20}$$

Similarly, the perturbation of the total kinase activity (Eq. S4) gives

$$\Delta A_{tot}^* = \left(1+\theta_b\right)\Delta A^* + \theta_c\,\Delta\varepsilon_{bp} \tag{S21}$$

In equation (S18), the time scale τ_{GK} is the same as the relaxation time scale of Goldbeter and Koshland's covalent modification system (30), whereas g_b is the rate of change of the methylation level of the system in response to a perturbation in the concentration of CheB-P. For the system without the CheB-P feedback loop, $\Delta\varepsilon_{bp}$ is zero.

The linear perturbation of the kinase activity ΔA^* contains two terms (Eq. (8)):

$$\Delta A^*(t) = \underbrace{\sum_{m=0}^{m_{\max}}\Delta a_m(t)\,\overline{X}_m}_{\Delta A_{input}^*} + \underbrace{\sum_{m=0}^{m_{\max}}\overline{a}_m\,\Delta X_m(t)}_{\Delta A_{adapt}^*} \cong \Delta A_{input}^* + \beta\,\Delta M \tag{S22}$$

The first term results from the perturbation in the external concentration of ligand whereas the second term describes the change in kinase activity due to perturbations in the methylation level of the receptors. To keep our analysis independent from various models of receptors, we use directly $\Delta A_{input}^* = \sum_m\Delta a_m\,\overline{X}_m$ as the input of the adaptation

module without detailing the relationship of Δa_m to changes in ligand concentration. The term, $\Delta A^*_{\text{adapt}}$, represents the change in kinase activity due to small changes ΔX_m in the methylation levels of the receptors at constant external concentration of ligand, $\overline{L}$. Neglecting for simplicity the contributions from the receptor complexes bound to CheR and CheB-P, we have $\overline{A} + \overline{A}^* \cong 1$, $\sum_m \overline{X}_m \cong 1$, $\sum_m \Delta X_m \cong 0$, and we can interpret ΔX_m as the perturbation of the distribution $\overline{X}_m$ of methyl groups at steady state (Eq. S16). Expanding the activation probability $\overline{a}_m = \overline{a}(m) = a(m, \overline{L})$ around the mean methylation at steady state, $\overline{a}_m = \overline{a}(\overline{M}) + \overline{a}'(\overline{M})(m - \overline{M}) + ...$, and inserting in Eq. S22, we obtain

$$\Delta A^*_{\text{adapt}} = \overline{a}'(\overline{M}) \Delta \langle (m - \overline{M})^1 \rangle + \overline{a}''(\overline{M}) \Delta \langle (m - \overline{M})^2 \rangle / 2 + \overline{a}'''(\overline{M}) \Delta \langle (m - \overline{M})^3 \rangle / 3! + ...$$

where $\Delta \langle (m - \overline{M})^k \rangle = \sum_m (m - \overline{M})^k \Delta X_m$ is the perturbation in the k-th moment of the distribution of methyl groups. Keeping only the contribution from the perturbation in the mean methylation level $\Delta M = \Delta \langle m - \overline{M} \rangle = \sum_m m \Delta X_m$ and neglecting the contributions from small changes in the second and higher moments of the distribution of methyl groups, we arrive at the following expression for the perturbation of the mean kinase activity: $\Delta A^*_{\text{adapt}} = \Delta \langle a(m, \overline{L}) \rangle \cong \beta \Delta M$. Here $\beta = \overline{a}'(\overline{M}) = (\partial a / \partial m)_{L=\overline{L}, m=\overline{M}}$ is the gain in kinase activity for a small change in methylation level around steady state. This linear approximation simplifies the analytical treatment while capturing the basic dependence of the kinase activity on methylation level as established by biochemistry data (16, 20, 31). In the simple case where $a_m = m / m_{\max}$ the approximation becomes exact and from Eq. S22 we have immediately $\Delta A^*_{\text{adapt}} = \sum_m a_m \Delta X_m = \sum_m m \Delta X_m / m_{\max} = \Delta M / m_{\max}$. When considering the *slow* stochastic fluctuations in non-stimulated cell we have: $\delta A^* = \delta A^*_{input} + \beta \delta M \cong \beta \delta M$.

Eliminating ΔM from (S18) and performing the linear expansion of equations (S6–S8) we obtain the following system of linear equations:

$$\frac{d}{dt} \begin{pmatrix} \Delta A^* \\ \Delta \varepsilon_{bp} \\ \Delta Y_p \\ \Delta A_p \end{pmatrix} = - \underbrace{\begin{pmatrix} \beta \tau_{GK}^{-1} & \beta g_b & 0 & 0 \\ -d_b \theta_b & a_b \overline{A}_p + d_b(1-\theta_c) & 0 & -a_b \overline{B} \\ 0 & 0 & a_y \overline{A}_p + d_y & -a_y \overline{Y} \\ k_p(\overline{A}_p - 1)(1+\theta_b) & k_p(\overline{A}_p - 1)\theta_c - a_b \overline{A}_p & -a_y \overline{A}_p & k_p \overline{A}^*_{tot} + a_b \overline{B} + a_y \overline{Y} \end{pmatrix}}_{\Gamma} \begin{pmatrix} \Delta A^* \\ \Delta \varepsilon_{bp} \\ \Delta Y_p \\ \Delta A_p \end{pmatrix} + \frac{d}{dt} \begin{pmatrix} \Delta A^*_{input} \\ 0 \\ 0 \\ 0 \end{pmatrix} \quad \text{(S23)}$$

The matrix Γ is the relaxation matrix of the system. For the parameter values in Table S1 the eigenvalues of Γ are all real and positive, ensuring that the steady state is stable. The rate of relaxation of the system towards equilibrium is governed by the smallest eigenvalue of Γ, which we calculate numerically using the Eigenvalues[] routine from the Mathematica 5.2 software. The inverse of the smallest eigenvalue of Γ is the relaxation time of the system τ_a. We plot τ_a as function of [CheR] and [CheB] in Figure 2.

We can calculate an analytical expression for the relaxation time of the system with the CheB-P feedback loop if we further simplify equation (S23). We take into account the fact that the methylation-demethylation reactions are much slower than the reaction involved in the phosphorylation cascade. Thus, on the long time scales relevant for the methylation-demethylation process equations (S6-S8) are at quasi-steady state and we can solve them to obtain ε_{bp} as a function of A^*, ε_b and ε_y

$$\varepsilon_{bp} = \varepsilon_{bp}(A^*, \varepsilon_b, \varepsilon_y) \tag{S24}$$

Notice that there is no explicit dependency on ε_r in this equation. The dependency of ε_{bp} on ε_r exists only via the dependency of A^* on ε_r. The total concentration of CheB and CheY proteins do not vary as a function of time. Thus, the relative change in time of phosphorylated CheB, $\Delta\varepsilon_{bp}$, as a function of the relative change in time of the kinase activity ΔA^* is

$$\frac{\Delta\varepsilon_{bp}}{\overline{\varepsilon}_{bp}} = \mu_a \frac{\Delta A^*}{\overline{A}^*} \tag{S25}$$

where $\mu_a = \partial \ln \overline{\varepsilon}_{bp} / \partial \ln \overline{A}^*$. In the appendix we derive an approximate expression for μ_a. Inserting (S25) into the first line of (S23) yields the relaxation time for the adaptation system with the CheB-P feedback loop:

$$\tau_a^{-1} = \beta\left(\tau_{GK}^{-1} + \frac{g_b \overline{\varepsilon}_{bp}}{\overline{A}^*}\mu_a\right) = \beta\left[\tau_{GK}^{-1} + \overline{b}\mu_a\left(1 + \frac{k_r}{k_b}\frac{\theta_r}{1+\theta_r}\right)\right] \tag{S26}$$

τ_{GK} and g_b are defined in equation (S18). In the next subsection (SI Sec. 2.4) we analyze how the relaxation time depends on [CheR] and [CheB].

For the system without the CheB-P feedback loop the relaxation of the kinase activity decouples from the relaxation of the other variables and the perturbation equation for the kinase activity (S23) simply becomes

$$\frac{d}{dt}\Delta A^* = -\frac{\beta}{\tau_{GK}}\Delta A^* + \frac{d}{dt}\Delta A^*_{input} \tag{S27}$$

In signal control theory, equation (S27) is equivalent to a negative integral feedback loop (32). The relaxation time in this case is $\tau_a = \tau_{GK} / \beta$ (Figure 2C). Multiplying equation

(S27) with $(1+\theta_b)$ yields equation (4) in the main text. The relaxation time τ_a is a function of the steady state activity $\overline{A}^*$ but does not depend explicitly on the activation probabilities $a_m(L)$. Therefore, like the steady state, τ_a is independent of the ambient concentration of ligand in the external medium. Thus, adaptation should be independent from the ambient concentration of ligand.

2.4 Analysis of the relaxation time of the adaptation module

In this section we analyze how the relaxation time varies as a function of the total intracellular concentrations of CheR (ε_r) and CheB (ε_b). If we take the total derivative of the conservation of mass equation *at steady state* (Eq. (2) in main text) we obtain (compare with (S19):

$$(1+\theta_r)d\overline{A} + \frac{\overline{r}\,\overline{A}}{k_r}d\ln\varepsilon_r + (1+\theta_b)d\overline{A}^* + \frac{\overline{b}\,\overline{A}^*}{k_b}d\ln\overline{\varepsilon}_{bp} = 0 \qquad (S28)$$

Similarly, the total derivative of the equilibrium condition $\overline{r}\,\overline{A} = \overline{b}\,\overline{A}^*$ (Eq. 1 in main text) yields:

$$k_r\theta_r\,d\overline{A} + \overline{r}\,\overline{A}\,d\ln\varepsilon_r + k_b\theta_b\,d\overline{A}^* + \overline{b}\,\overline{A}^*\,d\ln\overline{\varepsilon}_{bp} = 0 \qquad (S29)$$

Eliminating $d\overline{A}$ from (S28) and (S29) we get

$$\tau_{GK}^{-1}d\overline{A}^* = \frac{\overline{r}\,\overline{A}}{1+\theta_r}d\ln\varepsilon_r - \frac{\overline{b}\,\overline{A}^*}{1+\theta_r}\left[1+\theta_r\left(1+k_r/k_b\right)\right]d\ln\overline{\varepsilon}_{bp} = 0 \qquad (S30)$$

The total derivative of the CheB-P feedback relation at steady state, equation (S24), yields

$$d\ln\overline{\varepsilon}_{bp} = \mu_a\,d\ln\overline{A}^* + \mu_b\,d\ln\varepsilon_b \qquad (S31)$$

where $\mu_b = \partial\ln\overline{\varepsilon}_{bp}/\partial\ln\varepsilon_b$. Finally, inserting (S31) in (S30) and using (S26) we obtain an equation for the total derivative of the steady state kinase activity of free receptor complexes

$$d\overline{A}^* = \frac{\beta\overline{b}\,\overline{A}^*\tau_a}{(1+\theta_r)}\left\{d\ln\varepsilon_r - \mu_b\left[1+\theta_r\left(1+k_r/k_b\right)\right]d\ln\varepsilon_b\right\} \qquad (S32)$$

12

The relaxation time τ_a is defined in (S26). Equation (S32) tells us how the relaxation time depends on the gradient of the kinase activity. For fixed CheB concentration we have

$$\tau_a(\varepsilon_r) = (1+\theta_r)\ \frac{1}{\beta\overline{b}}\left(\frac{\partial \ln \overline{A}^*}{\partial \ln \varepsilon_r}\right)_{\varepsilon_b} \cong \frac{1}{\beta\overline{b}}\left(\frac{\partial \ln \overline{A}^*}{\partial \ln \varepsilon_r}\right)_{\varepsilon_b} \tag{S33}$$

while for fixed CheR concentration we have

$$\tau_a(\varepsilon_b^{-1}) = \frac{1+\theta_r}{1+\theta_r\left(1+k_r/k_b\right)}\ \frac{1}{\beta\overline{b}\,\mu_b}\left(\frac{\partial \ln \overline{A}^*}{\partial \ln \varepsilon_b^{-1}}\right)_{\varepsilon_r} \cong \frac{1}{\beta\overline{b}\,\mu_b}\left(\frac{\partial \ln \overline{A}^*}{\partial \ln \varepsilon_b^{-1}}\right)_{\varepsilon_r} \tag{S34}$$

The approximations in (S33) and (S34) result after neglecting the small amount of receptors bound to CheR and CheB-P. This simplification is valid as long as $\theta_r = \varepsilon_r K_r/(K_r + \overline{A})$ is much smaller than one, which is well satisfied for physiologically relevant values of [CheR] ($\varepsilon_r = 0.03$ and K_r is of order 10^{-1} or smaller; Table 1).

In Figure 2 we plotted the relaxation time as a function of ε_r and ε_b^{-1} for the system with and without the CheB-P feedback loop. Here we analyze the main features of these curves in the light of equations (S33) and (S34). When plotted as a function of ε_r, the derivative in equation (S33) resembles a deactivation curve that is maximum and bounded for small values of ε_r and zero for large values of ε_r. The other factor that determines the relaxation time is the inverse rate of demethylation $\overline{b}^{-1} = (K_b + \overline{A}^*)/(k_b\overline{\varepsilon}_{bp})$. From the derivative of $\overline{b}^{-1}$ with respect to $\ln \varepsilon_r$,

$$\left(\frac{\partial \ln \overline{b}^{-1}}{\partial \ln \varepsilon_r}\right)_{\varepsilon_b} = \frac{\overline{A}^* - \left(K_r + \overline{A}^*\right)\mu_a}{k_b\varepsilon_{bp}}\underbrace{\left(\frac{\partial \ln \overline{A}^*}{\partial \ln \varepsilon_r}\right)_{\varepsilon_b}}_{\geq 0} \tag{S35}$$

we see that the slope of the relaxation time as function of ε_r depends on the strength of the CheB-P feedback loop. When the CheB-P feedback loop is weak ($\mu_a \approx 0$) the inverse rate of demethylation $\overline{b}^{-1}$ increases monotically from $K_b/(k_b\varepsilon_b)$ to $(K_b+1)/(k_b\varepsilon_b)$ as a function of ε_r. Therefore, $\tau_a(\varepsilon_r)$ peaks within the transition region of the kinase activation curve (Fig. 2C) as expected for a covalent modification cycle with a Hill coefficient larger than one (30, 33-35). For a stronger feedback loop, the slope of the relaxation time as a function of ε_r changes sign whenever

$$\mu_a = \frac{\overline{A}^*}{K_r + \overline{A}^*} \tag{S36}$$

At that value of ε_r the profile of $\tau_a(\varepsilon_r)$ exhibits a local minimum (Fig. 2D). Finally, for very strong CheB-P feedback loop ($\mu_a > 1/(1+K_r)$) the derivative of $\overline{b}^{-1}$ is always negative and the relaxation time is a decreasing function of ε_r everywhere. The profile of the noise in kinase activity $\sigma_a^2 \cong \tau_a \beta^2 \overline{b} \, \overline{A}^* / N$ is similar to that of τ_a with the exception that at low concentration of CheR, the noise becomes zero because of the pre-factor $\overline{b} \, \overline{A}^*$.

The profile of the relaxation time as a function of ε_b^{-1} for fixed concentration of CheR is described by equation (S34). Because ε_r and ε_b are much smaller than one (Table 1) we can neglect the receptor complexes bound to CheR and CheB-P in the mass conservation and therefore the steady state of the kinase activity $\overline{A}^*$ is a function of $\alpha = k_r \varepsilon_r / k_b \varepsilon_{bp}$ only. Thus, $\partial \ln \overline{A}^* / \partial \ln \varepsilon_r \approx -\partial \ln \overline{A}^* / \partial \ln \varepsilon_{bp} = -\partial \ln \overline{A}^* / \partial \ln \varepsilon_b / \mu_b$ and the differences between the profiles of $\tau(\varepsilon_r)$ and $\tau(\varepsilon_b^{-1})$ only depend on the differences between the profiles of $\overline{b}^{-1}(\varepsilon_r)$ and $\overline{b}^{-1}(\varepsilon_b^{-1})$. For a fixed value of ε_r, the inverse rate of demethylation $\overline{b}^{-1}$ as a function of ε_b^{-1} grows monotonically from zero to the maximal value $(K_b + 1)/(k_b \varepsilon_b)$. Thus the profile of the relaxation time as a function of ε_b^{-1} for fixed value of ε_r is a peak that decays to zero at both large and small values of ε_b^{-1}.

2.5 Stochastic fluctuations.

We calculate the strength of the stochastic fluctuations δA^* within a non-stimulated cell using the linear noise approximation (36-38). We first calculate the stochastic fluctuations $\delta M(t)$ of the methylation level of the free receptors about the steady state $\overline{M}$. We assume Poisson statistics for the individual methylation and demethylation steps. Thus, the contribution of the methylation $X_{m-1} \xrightarrow{r(1-a_{m-1})} X_m$ and demethylation $X_m \xrightarrow{b a_m} X_{m-1}$ reactions to the rate of change of the fluctuations $\delta M(t)$ is $\sqrt{(\overline{r}(1-\overline{a}_{m-1})\overline{X}_{m-1} + \overline{b}\,\overline{a}_m \overline{X}_m)/N} \, \delta \eta_m = \sqrt{2\overline{b}\,\overline{a}_m \overline{X}_m / N} \, \delta \eta_m$, where $\delta \eta_m$ is an independent source of white noise and N is the total number of receptor complexes in the system. Summing up the contributions from all the methylation and demethylation reactions we obtain the following stochastic differential equation for the time evolution of δM:

$$\frac{d}{dt}\delta M = -\frac{1}{\tau_{GK}}\delta A^* - g_b\,\delta\varepsilon_{bp} + \sqrt{\frac{2\overline{b}\,\overline{A}^*}{N}}\,\delta\eta_a \qquad (S37)$$

The last term in equation (S37) is a source term, representing the stochastic fluctuations due to the methylation-demethylation reactions. The rest of the equation is exactly the same as in equation (S18). Similar to equation (S22) we have the relation $\delta A^* = \delta A^*_{input} + \beta\,\delta M \cong \beta\,\delta M$ which together with equation (S37) yields an equation for the stochastic fluctuations δA^* of the activity of free receptors:

$$\frac{d}{dt}\delta A^* = -\frac{\beta}{\tau_{GK}}\delta A^* - \beta\,g_b\,\delta\varepsilon_{bp} + \sqrt{\frac{2\beta^2\overline{b}\,\overline{A}^*}{N}}\,\delta\eta_a \qquad (S38)$$

Equation (2) in the main text follows easily from Eq. (S38) when we neglect the CheB-P feedback loop ($g_b = 0$) and take into account the receptor-enzymes compounds. Applying, in a similar way, the linear noise approximation to equations (S6-S8) and including equation (S38) we obtain the following equation for the matrix C of the covariances of the fluctuations (δA^*, $\delta\varepsilon_{bp}$, δY_p, δA_p) within the system (36):

$$\frac{d}{dt}C = -\Gamma C - C\Gamma^T + D \qquad (S39)$$

where the diffusion matrix for the system is

$$D = \frac{1}{N}\begin{pmatrix} 2\beta^2\overline{b}\,\overline{A}^* & 0 & 0 & 0 \\ 0 & 2d_b\overline{B}_b & 0 & -d_b\overline{B}_p \\ 0 & 0 & 2d_y\overline{Y}_p & -d_y\overline{Y}_p \\ 0 & -d_b\overline{B}_p & -d_y\overline{Y}_p & a_b\overline{B}+k_p\overline{A}^*_{tot}+a_y\overline{Y} \end{pmatrix} \qquad (S40)$$

The elements of the matrix D represent the strength of the stochastic fluctuations associated with the individual reactions within the system (36-38). N is the total number of receptor complexes within the system. At steady state equation (S39) yields the Lyapunov matrix equation

$$\Gamma\overline{C} + \overline{C}\,\Gamma^T = D \qquad (S41)$$

which follows directly from the fluctuation dissipation theorem (39). We solve (S41) using the routine NSolve[] from the Mathematica 5.2 software to obtain the stationary covariance matrix $\overline{C}$. Finally, the steady state variance of the fluctuations in the total kinase activity $\sigma_a^2 = \left\langle \delta A_{tot}^* \, \delta A_{tot}^* \right\rangle$ follows easily from equation (S21):

$$\sigma_a^2 = \begin{pmatrix} 1+\theta_b & \theta_c & 0 & 0 \end{pmatrix} \overline{C} \begin{pmatrix} 1+\theta_b \\ \theta_c \\ 0 \\ 0 \end{pmatrix} \tag{S42}$$

For the system without the CheB-P feedback loop, the strength of the white noise associated with the methylation demethylation reactions in equation (2) is $\sqrt{D_a}$ where

$$D_a = \beta^2 \, \underbrace{\frac{\left(1+\theta_b\right)^2 \, 2\,\overline{b}\,\overline{A}^*}{N}}_{D_{GK}} \tag{S43}$$

Here $\sqrt{D_{GK}}$ is the strength of the random fluctuations associated with the two enzymatic reactions within the covalent modification system studied by Goldbeter and Koshland (30, 33). The variance of the fluctuations in the total kinase activity is then

$$\sigma_a^2 = \frac{\tau_a \, D_a}{2} = \beta \, \sigma_{GK}^2 \tag{S44}$$

where σ_{GK}^2 is the variance of the spontaneous fluctuations for the system studied in refs. (30, 33):

$$\sigma_{GK}^2 = \frac{\tau_{GK} \, D_{GK}}{2} \tag{S45}$$

The equations (S41), (S44) and (S45) are all directly inferred from the general relation between fluctuations and dissipation (11-13).

2.6 Spectral analysis

Taking the Fourier transform of equation (S39) we obtain the power spectrum matrix of the fluctuations $(\delta A^*, \, \delta\varepsilon_{bp}, \, \delta Y_p, \, \delta A_p)$ around the steady state (37, 39):

$$S(\omega) = 2\operatorname{Re}\left[\left(\Gamma + i\omega\right)^{-1} D \left(\Gamma^T - i\omega\right)^{-1}\right] \qquad (S46)$$

The power spectrum of the fluctuations in [CheY-P] is the third element along the diagonal in the matrix S. We plot the power spectrum of CheY-P in Figure 3.

It is interesting to calculate the frequency response of the chemotaxis system when we neglect the effects of the CheB-P negative feedback loop and assume quasi-equilibrium between phosphorylated and unphosphorylated kinases. For this simpler case, the linear perturbation analysis of the chemotaxis system (equations (3), (4) and (A1-A3)) yields the following system of equations for the stochastic fluctuations in total kinase activity and in the concentration of CheY-P around steady state:

$$\frac{d}{dt}\delta A^*_{\text{tot}} = -\frac{1}{\tau_a}\delta A^*_{\text{tot}} + \sqrt{D_a}\,\delta\eta_a + \frac{d}{dt}\delta A^*_{input} \qquad (S47)$$

$$\frac{d}{dt}\delta Y_p = -\underbrace{\left(a_y \overline{A}_p^2 + d_y\right)}_{\tau_y^{-1}}\delta Y_p \;+\; \sqrt{D_y}\,\delta\eta_y \;+\; \underbrace{k_p\left(\frac{a_y \overline{A}_p \overline{Y}}{k_p \overline{A}^*_{tot}}\right)^2}_{g_y}\delta A^*_{\text{tot}} \qquad (S48)$$

Here δA^*_{input} represents the fluctuations in the input of the system to fluctuations in the binding-unbinding of external ligand. In Eq (S48) τ_y is the relaxation time of the response regulator module (Fig. 1). Unlike τ_a, τ_y is independent from the level of CheR and CheB-P within the cell. D_y represents the strength of the stochastic fluctuations in the phosphorylation cascade, g_y is the gain and $\delta\eta_y$ is white noise. Taking the Fourier transform of Eqs (S47) and (S48) we obtain the power spectra of δA^*_{tot} and δY_p respectively:

$$S_{\delta A^*_{\text{tot}}}(\omega) \;=\; \frac{\tau_a^2 \omega^2}{1+\tau_a^2 \omega^2}\left(S_{\delta A^*_{input}}(\omega) \;+\; \frac{2D_a}{\omega^2}\right) \qquad (S49)$$

$$S_{\delta Y_p}(\omega) \;=\; \frac{\tau_y^2 g_y^2}{1+\tau_y^2 \omega^2}\left(S_{\delta A^*_{\text{tot}}}(\omega) \;+\; \frac{2D_y}{g_y^2}\right) \qquad (S50)$$

Eq. (S49) reveals that the adaptation module is a high-pass filter with cutoff frequency τ_a^{-1}. The response regulator module (S50) is a low-pass filter with cutoff frequency τ_y^{-1}.

3. Sensitivity of the adaptation module

3.1 Covalent modification cycles (primer)

Covalent modification systems have emerged as an alternative mechanism to allostery to amplify signals in biological systems (30, 33-35, 40-42). Recent experiments have found sensitive covalent modification mechanisms in the turning on or off of the cell cycle in oocytes (43), the conversion of a graded MAPK activation into an all-or-none switch that governs the development of *Drosophila* embryonic ventral ectoderm (44). Covalent modification systems (30, 42) often consist of two enzymes that reversibly modify one substrate between an inactive and an active state (Figure S2). When the corresponding Michaelis-Menten constants are smaller than substrate concentration, the enzymes operate near saturation and the system departs from hyperbolic (Michaelis-Menten) sensitivity. The fraction of modified substrate becomes a sigmoidal function of the ratio, α, of the maximal enzymatic velocities. The sharpness of the sigmoidal curve depends on the ratio of the Michaelis-Menten constants to the concentration of substrate $K_m/[Substrate]$. The smaller the values of $K_m/[Substrate]$, the sharper the transition between all inactive to all active substrate. For values of α outside of the transition region of the sigmoidal curve, the enzymatic velocities are asymptotically insensitive to changes in the substrate. The system is blocked in one state or the other, with substrate molecules mostly modified or unmodified. By contrast, when the relative velocities of the two converting enzymes (the parameter α) tune the system within the transition region of the sigmoidal curve, the system becomes sensitive to stochastic variations in the catalytic rates of substrate modification (30). This regime is characterized by large fluctuations in the amount of modified substrate associated with large characteristic time scales (33, 34, 38). Within the transition region, the enzymatic rates vary rapidly as function of the fractions of unmodified and modified substrates. Thus, even though the enzymes are working near saturation ($K_m/[Substrate]$ smaller than one), we must retain the full nonlinear form of the Michaelis-Menten rates (in our case r and b defined in Eq. (1)). Finally, when the ratio of maximal enzymatic velocities, α, is tuned within the transition region of the sigmoidal curve, the system is sensitive not only to small variations in α but also to small changes in the relative amount of modified and unmodified substrate.
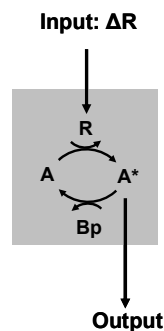

Figure S2. Covalent modification network (30, 33). Unlike in the chemotaxis system (Figure 1A main text), the input signal is one of the modifying enzymes. The system works as an amplifier.

3.2 The sensitivity of the adaptation module

In SI Sec. 2 above, we showed that at steady state the concentration of receptor complexes $\bar{A}$ obeys the equation derived by Goldbeter and Koshland to describe the fraction of unmodified proteins as function of the ratio of maximal enzymatic speeds (compare Eq. (S15) with the caption of Fig. 3 on page 6842 of (30)). Thus, the structural design of the adaptation module in chemotaxis and the architecture of the simpler covalent modification cycle are similar. Moreover, the relaxation time τ_a of the adaptation module and the variance σ_a^2 of the stochastic fluctuations in kinase activity are each proportional to their corresponding values τ_{GK} and σ_{GK}^2 in a covalent modification cycle (30). Consequently, the adaptation module in the chemotaxis system (Figure 1) should share some of the properties of the futile cycle studied by Goldbeter and Koshland (Figure S2).

The sensitivity of a covalent modification cycle depends on the ratios of the Michaelis-Menten constants to the concentration of substrate. We therefore investigated the dynamics of adaptation for different values of the normalized Michaelis-Menten constants K_r and K_b between 10^{-2} and 1. Recent biochemical data (45) provide the (normalized) intracellular concentrations of CheR and CheB proteins: $\varepsilon_r = 0.03$, $\varepsilon_b = 0.053$. Taking into account these constraints we find that our model best reproduces measurements from single cells and populations when K_r and K_b are of order 10^{-1}: $K_r = 0.132$ and $K_b = 0.176$ (Table S1). If instead we increase $(K_r, K_b \approx 10^{-2})$ or decrease $(K_r, K_b \approx 1)$ the values of the Michaelis-Menten constants we find that we cannot simultaneously reproduce the behavioral variability measured (1) in single cell measurements of wild type and CheR mutant bacteria (Figures 3 and S3). For K_r and K_b of order 10^{-2} (5 times smaller than in Table S1), the system is ultra-sensitive. The peak of the relaxation time is narrow with a large amplitude (Figure S3A), indicative of a very sharp transition between a regime where the kinases are fully inactive to a regime where the kinases are fully active (plot not shown). In contrast, for values of K_r and K_b that are of order 1 (10 times larger than in Table S1), the system works in the regime of first order kinetics: the activation curve of the kinase activity versus [CheR] is hyperbolic and the peaking of the relaxation time disappears (Figure S3A). In this regime the power spectrum of the flutuations in CheY-P is nearly insensitive to changes in the concentration of CheR, in contradiction with experimental data (1).

An important feature of the power spectra in Fig S3 ($K_r = 0.132$) is the presence for wild-type cells of a growing profile with a knee frequency at very long time scales. Recent experimental measurements from mutant cells either with deleted signaling pathway (*ΔcheB, ΔcheZ, ΔcheY,* complemented with *cheYD13K*) or mutants with receptors that have fixed intermediate methylation level (strain deleted for *cheR, cheB, tsr, tar, tap, trg* and transformed with Tsr mutant receptors with QQQQE methylation sites) do not exhibit large fluctuations at long time scales like in wild type cells with comparable CW bias (1). These measurements clearly indicate that the source of the large fluctuations is the slow methylation-demethylation process (the faster phosphorylation

19
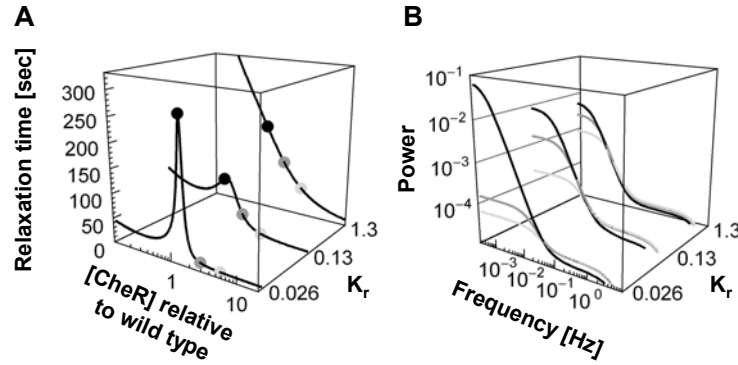
Figure S3: (**A**) Relaxation times as a function of [CheR] relative to wild-type level, for values of K_r and K_b that are 0.2, 1 and 10 times the values listed in Table S1 and used in the main text. The circles indicate factors of two in [CheR]. For K_r=0.13 and 1.3, black corresponds to wild-type. For K_r=0.026, black corresponds to the maximum relaxation time. (**B**) Same power spectra as in Figure 3. Values of K_r and K_b that are 1/5, 1 and 10 times those listed in Table 1. The different colors correspond to different concentration of CheR increasing in factors of two. The values of [CheR] are the same as for the circles in panel **A.**

cascade gives rise to the knee frequency visible at much shorter time scales) and our model provides the corresponding quantitative explanation.

Recent biochemical data measurements of the concentration of chemotactic proteins in *E. coli* found about 17μM of the abundant receptors Tar and Tsr for 5.3μM of kinase CheA (long) (45). This suggests a structural arrangement of approximately three receptors per kinase. Measurements of the catalytic activity of CheR and CheB-P in receptor monomers gave $K_{mr} \cong 2.1\,\mu\text{M}$ (46) and $K_{mb} \cong 2.8\,\mu\text{M}$ for CheB-P (47). Thus, the ratios of Michaelis-Menten constants to substrate concentration for receptor monomers are approximately of order 10^{-1} (K_{mr} /[Substrate] $\cong 0.12$ for CheR and $\cong 0.17$ for CheB-P), indicating that the individual methylation-demethylation cycles of the receptors are working outside of the region of first-order kinetics (see e.g. Figure 3 on page 6842 of (30)). There are no measurements of the Michaelis-Menten constants K_r and K_b in receptor complexes that involve several receptor monomers. One way of estimating these values from the current biochemical data is to use the measured stochiometry of three receptor dimmers per dimmer of kinase. The affinity of receptor complexes to enzymes are therefore about six times those of receptor monomers to enzymes. But the concentration of receptor complexes is also six times smaller than that of monomers. Thus, Michaelis-Menten constants and substrate concentration scale similarly with respect to the number of receptors within a receptor complex. These scaling factors cancel out when we take the ratio of Michaelis-Menten constants to substrate concentration. We conclude that the current biochemical data provides a lower bound (10^{-1}) for the effective normalized Michaelis-Menten constants used in our model. This value is in line with recent models of bacterial chemotaxis (17, 19, 20). In fact, most

models assume even smaller values for K_r, making the system even more sensitive and noisy (See SI Table S2 in Sec 4 below).

Description	Symbol	Dimensional Units	Normalized	Reference
CheA concentration		5.3 μM	1	(45)
CheY concentration	ε_y	9.7 μM	1.830	(45)
CheR concentration	ε_r	0.16 μM	0.030	(45)
CheB concentration	ε_b	0.28 μM	0.053	(45)
Receptor concentration (Tar+Tsr)		17 μM	3.2	(45)
CheR Michaelis-Menten (methylation of a receptor complex)	K_r	0.39 μM	0.13	this work
CheB-P Michaelis-Menten (demethylation of a receptor complex)	K_b	0.54 μM	0.18	this work
CheR catalytic rate	k_r	0.75 s^{-1}	0.75 s^{-1}	this work
CheB-P catalytic rate	k_b	0.6 s^{-1}	0.6 s^{-1}	this work
CheA autophosphorylation rate	k_p	23.5 s^{-1}	23.5 s^{-1}	(48), 27 s^{-1}
CheY phosphorylation rate	a_y	100 μM^{-1} s^{-1}	530 s^{-1}	(49)
CheY-P dephosphorylation rate	d_y	30 s^{-1}	30 s^{-1}	(29)
CheB phosphorylation rate	a_b	10 μM^{-1} s^{-1}	53 s^{-1}	(49, 50)
CheB-P dephosphorylation rate	d_b	1 s^{-1}	1^{-1}	(19)
Cell volume		1.41×10^{-15} L		
	m_{max}	4	4	

Table S1: Model parameters. The protein concentrations are from (45). We normalized the concentrations with the intracellular concentration of CheA (long). When we consider the model without CheB-P feedback loop, the concentration of modifying enzyme CheB-P is constant and equal to its wild type value in the full model: $\varepsilon_{bp} = 0.04$. We adjusted the catalytic rates of CheR and CheB-P as well as the normalized Michaelis-Menten constants to fit the power spectra from single cells measurements in wild type and CheR mutants (1) (see the main text).

4. Alternative models and validation with numerical simulations

4.1 Parameter values from other models

In Table S2 we list the parameter values from published models of chemotaxis (17, 19, 20). In all these models, the normalized Michaelis-Menten constants for the enzymes CheR and CheB-P are smaller than one. Figures S4 show that the adaptation module in Bray and collaborators model (17) is working outside of the regime of first-order kinetics. We validate our analytical stochastic model of adaptation with stochastic numerical simulations of the bacterial chemotaxis system using StochSim (17) (Figure S4C).

Description	Symbol	Morton-Firth et al. (17)		Rao et al. (51)		Kolman et al. (20)	
		Dimensional	Normalized	Dimensional	Normalized	Dimensional	Normalized
CheA concentration		5 μM	1	5 μM	1	5.3 μM	1
CheY concentration	ε_y	18 μM	3.6	17.9 μM	3.58	9.7 μM	1.83
CheR concentration	ε_r	0.235 μM	0.047	0.3 μM	0.06	0.16 μM	0.03
CheB concentration	ε_b	2.27 μM	0.454	2. μM	0.4	0.28 μM	0.053
CheR Michaelis-Menten	K_r	0.364 μM	0.0728	0.251 μM	0.050	0.099 μM	0.019
CheB-P Michaelis-Menten	K_b	1.405 μM	0.281	5.5 μM	1.1	2.5 μM	0.47
CheR catalytic rate	k_r	0.819 s^{-1}	0.819 s^{-1}	0.255 s^{-1}	0.255 s^{-1}	0.39 s^{-1}	0.39 s^{-1}
CheB-P catalytic rate	k_b	0.155 s^{-1}	0.155 s^{-1}	0.5 s^{-1}	0.5 s^{-1}	6.3 s^{-1}	6.3 s^{-1}
CheA autophosphorylation rate	k_p	15.5 s^{-1}	15.5 s^{-1}	50 s^{-1}	50 s^{-1}	50 s^{-1}	50 s^{-1}
CheY phosphorylation rate	a_y	3 μM^{-1} s^{-1}	15 s^{-1}	100 μM^{-1} s^{-1}	500 s^{-1}	100 μM^{-1} s^{-1}	530 s^{-1}
CheY-P dephosphorylation rate	d_y	14.15 s^{-1}	14.15 s^{-1}	30.1 s^{-1}	30.1 s^{-1}	30.1 s^{-1}	30.1s^{-1}
CheB phosphorylation rate	a_b	3 μM^{-1} s^{-1}	15 s^{-1}	30 μM^{-1} s^{-1}	150 s^{-1}	3 μM^{-1} s^{-1}	15.9 s^{-1}
CheB-P dephosphorylation rate	d_b	0.35 s^{-1}	0.35 s^{-1}	1 s^{-1}	1 s^{-1}	1 s^{-1}	1 s^{-1}
Cell volume		1.4×10^{-15} L		1.4×10^{-15} L		1.4×10^{-15} L	
	$m_{\max}$	4	4	4	4	4	4

Table S2. Parameter values computed from other models of chemotaxis (17, 19, 20).
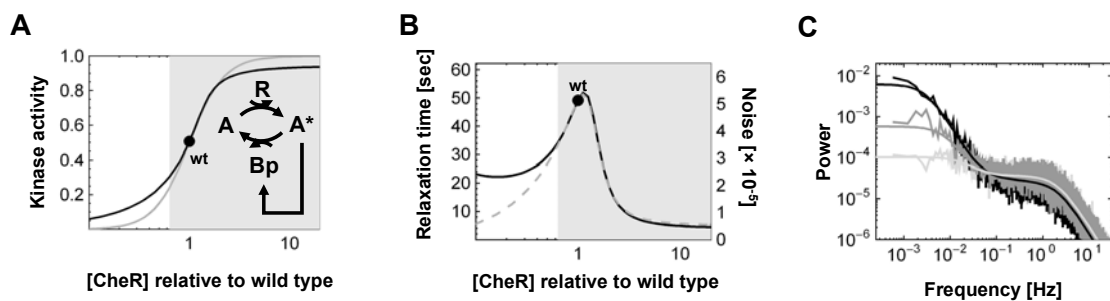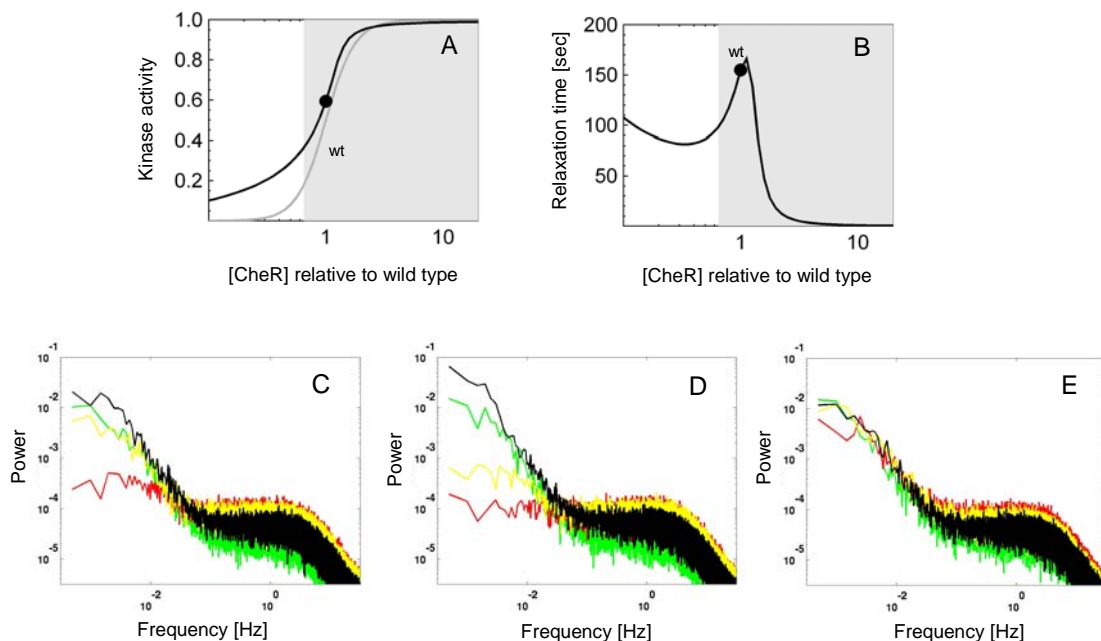
Figure S4. Same as Figures 2 and 3 in the main text but with parameter values as in (17) (Table S2). (**A**) (black) Total kinase activity A_{tot}^* as a function of [CheR] for a fixed wild type level of [CheB]. (grey) same without the CheB-P feedback loop. (**B**) Relaxation time τ_a (black) and variance σ_a^2 (grey) of the noise associated with the total kinase activity. (**C**) Power spectra of the fluctuations of output signal (CheY-P) from non-stimulated cells. One (black), two (grey) and four fold (light grey) wild-type levels of CheR for a fixed wild type level of [CheB]. (jagged lines) stochastic numerical simulation of the chemotaxis system.

4.2 Coarse-grain models of the methylation demethylation reactions

During the past decade, in vitro experiments have provided many details about the complicated process of methylation and demethylation of the receptors. Using purified solutions of isolated receptors in the absence of all other chemotaxis components found in living cells Wu et al. (52) showed that there exists a tethering site on Tsr and Tar receptors that is distinct from the sites of methylation, which helps recruit CheR to the receptor. Since the Wu paper, a series of papers have started to analyze in more details the complexity of the precise chemical action of CheR during the methylation process (53-56). For example, it was recently reported that the tethered CheR can methylate the receptors that are in the immediate vicinity in a complicated inter-dimmer process, defining an "assistance neighborhood"(57). Undoubtedly, as biochemical experiments become more sophisticated (58) and include a larger number of chemotaxis components, more complex biochemical mechanisms will emerge.

By contrast, the current models of chemotaxis use simplifying hypotheses that coarse-grain the underlying biochemical details to describe the biology of the full chemotaxis system obtained from experiments on living cells. Over the last decade, all the models of chemotaxis (including ours) that use the Barkai and Leibler activity-dependent feedback in the receptor modification system (15) have made the assumption that CheR binds the methylation sites of inactive receptors (17-21, 28, 59). This reaction network reproduces both the robust adaptation measured at the population level (60) and the nonlinear changes in relaxation time in single cells as a function of [CheR] (1) (Figures 2 and 3 in the main text and SI Fig S5C). We obtain similar results using the parameter values of the stochastic numerical model developed independently by Morton-Firth et al. (17) (Figure S4 and Table S2).

Figure S5: (**A-B**) Same as Figure 2 but with CheR always active (methylates both active and inactive receptor complexes) and parameters from Table S1. (**A**) (black) Total kinase activity A_{tot}^* as a function of [CheR] for a fixed wild type level of [CheB]; (grey) same without the CheB-P feedback loop. (**B**) Relaxation time τ_a as a function of [CheR] for a fixed wild type level of [CheB]. (**C-E**) Power spectrum of the spontaneous fluctuations in CheY-P for intracellular concentration of CheR corresponding to ½ (green), 1 (black), 2 (yellow) and 4 (red) fold the wild type level. (**C**) CheR binds the methylation site of inactive receptors only; (**D**) CheR interacts with the methylation sites irrespective of the activity of receptors; (**E**) only the catalytic step of the methylation reaction depends on receptor activity. The stochastic simulations (**C-E**) were performed with the stochastic simulator BioNetGen that uses a standard exact Gillespie algorithm to integrate the chemical master equations in time. Reaction rates in Table S1.

Another plausible simplification, also considered in Barkai and Leibler (15), is that neither the access to the methylation site nor the actual transfer of methyl group to the receptor depend on the activity of receptors. Figures S5A,B&D show that there are no qualitative differences between this case and the one presented in the main text.

The last simplifying possibility is that only the catalytic step of the methylation reaction depends on the receptor activity but not the binding of CheR. Under this condition, we found that the power spectra of the spontaneous fluctuations of the kinase activity are not sensitive to variations of [CheR] (Figure S5E). This behavior contradicts the measurements on single living cells in Ref. (1).

Figures S5C, S5D and S5E illustrate these 3 distinct simplifying assumptions, of which only the first two are compatible with the known biology of the chemotaxis system.
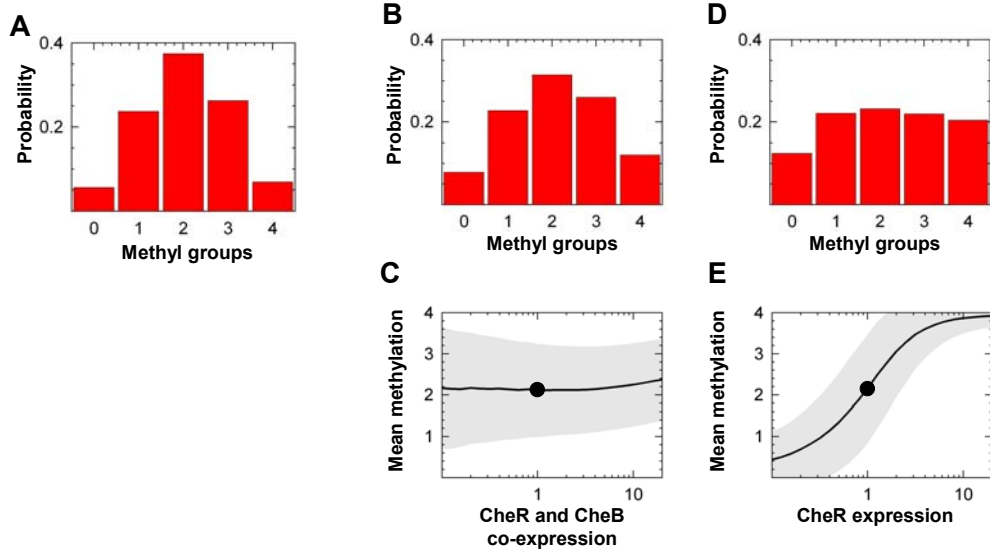
5. Distribution of [CheR] and [CheB] across a cell population.

The distribution of CheY proteins within a population of wild type cells was recently measured by (20). We generated the distributions of [CheR] and [CheB] using the Eq. (S17) of (20). For the distribution of [CheR] within the population, we used $x_r = \varepsilon_r \left(\lambda \mu_r + 0.2 \xi_{r2} \sqrt{\lambda \mu_r} \right)$ where ε_r is the average concentration of CheR, λ is the expression level relative to wild-type and μ_r is defined as $\mu_r = q_r \exp[0.2 \xi_{r1} \ln 10]$ with q_r chosen such that $\langle \mu_r \rangle = 1$. Similarly, for the distribution of [CheB] we used $x_b = \varepsilon_b \left(\lambda \mu_b + 0.2 \xi_{b2} \sqrt{\lambda \mu_b} \right)$ with $\mu_b = q_b \exp[0.2 \xi_{b1} \ln 10]$. The random variables ξ_{r1}, ξ_{r2}, ξ_{b1} and ξ_{b2} are normally distributed with mean zero and variance one. For the inset of Figure 2D we assumed that *cheB* was expressed on the chromosome deleted for *cheR* and that *cheR* was expressed from a low copy plasmid. When *cheR* and *cheB* were both expressed from the chromosome (Figure S6B and S6C) then $\mu_b = \mu_r$ (20).

6. Distribution of methyl groups

In the middle of the transition region in Figure 2B, $\overline{A} \cong \overline{A}^* \cong 0.5$ and the mean and standard deviations of the distribution (S17) are approximately $m_{max} / 2$ and $\sqrt{m_{max}} / 2$ respectively (Fig. S6A). Taking into account the receptor complexes bound to CheR and CheB-P does not change the distribution significantly because ε_r and ε_{bp} are much smaller than 1. Including the spontaneous fluctuations in kinase activity does not significantly modify the unimodal shape of the steady state distribution of methyl groups in a single cell either (stochastic simulations, data not shown).
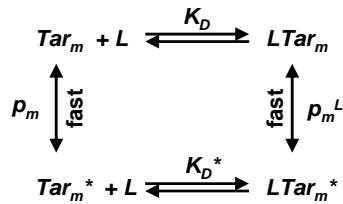
Because of the cell-to-cell variability of CheR and CheB concentrations within a bacterial population, the sensitivity of the adaptation mechanism to the ratio of the methylation and demethylation velocities should have a noticeable effect on the distribution of methylation levels within a *population* of cells. Taking into account the fact that the *cheR* and *cheB* genes are adjacent on the same operon (see SI Sec. 4), we find only small differences between the distribution of methyl groups in a single cell (Figure S6A) and the distribution of methyl groups across a population of wild type cells (Figure S6B). The resulting distribution is in agreement with earlier measurements (61). The fact that there are only small differences between Figures S6A and S6B illustrate the known reduction of independent variations between the expression of two adjacent genes on a multi-cistronic operon (20). The co-variation of CheR and CheB reduces the variations of the ratio α of methylation-demethylation velocities across the population (Figure S6C). In contrast, when *cheR* and *cheB* are expressed independently, (i.e. *cheR* on a plasmid and *cheB* constitutively on the chromosome), this robust aspect of the system breaks down. In this case, the distribution of methyl groups depends on the independent distributions of CheR and CheB (Figure S6D, E).

Figure S6. Distribution of the methyl groups. (**A**) Distribution of methyl groups in the steady state solution of the kinetic system for wild type levels of CheR and CheB ($\overline{X}_m$ from Eq. S15). (**B**) Distribution of methyl groups across a population of cells when *cheR* and *cheB* are co-expressed on the multi-cistronic operon *meche* at wild type levels (See SI Sec. 5 and ref. (20)). (**C**) Mean (black) plus-minus the standard deviation (grey) of the distribution of methylation groups across a population of cells as function of the level of expression relative to wild type. *cheR* and *cheB* are co-expressed as in **B**. (**D**) and (**E**) Same as (**B**) and (**C**) but expressing *cheR* and *cheB* separately as described in SI Sec. 5.

7. Probability of activation of a receptor complex

In the numerical simulations presented in Fig. 4 of the main text we use the same definition of the activation probability of a receptor complex $a_m(L)$ as in (1, 33). On the time scales relevant for the methylation and demethylation reactions ligand binding and receptor conformation changes operate at quasi-equilibrium. Ligand–receptor dissociation constant K_D depends on receptor activity but is independent of the methylation level. Schematically we have:

$$Tar_m + L \xrightarrow{\quad K_D \quad} LTar_m$$

$$p_m \Big\uparrow \text{fast} \qquad\qquad \text{fast} \Big\uparrow p_m^L$$

$$Tar_m^* + L \xrightarrow{\quad K_D^* \quad} LTar_m^*$$

where Tar_m and Tar_m^* represent inactive and active receptor complexes with m methyl groups, and K_D^* is the dissociation constant for active receptors. p_m and p_m^L ($m=0,\ldots4$)

are the probabilities of activation for free and ligand-bound receptors, respectively. Because of the assumption of quasi-equilibrium they satisfy the relation

$$\frac{K_D^*}{K_D} = \frac{p_m}{1-p_m} \frac{1-p_m^L}{p_m^L} \tag{S35}$$

We can express the activation probability of the kinase $a_m(L)$ as function of K_D, K_D^* and the 5 probabilities p_m:

$$a_m(L) = \left(1 + \frac{L+K_D}{L+K_D^*} \frac{K_D^*}{K_D} \frac{1-p_m}{p_m}\right)^{-1} \tag{S36}$$

We plot the probabilities $a_m(L)$ for L=0, 1, 10 and 100 μM aspartate using the same dissociation constants and p_m values as in (17) (Figure S7A). These are also the parameter values that we used for the numerical simulations plotted in Figure 4. Finally, we plotted in Figure S7B the probability of activation used by (20) that is based on measurements from (16). In all cases, for small concentrations of ligand, $a_m(L)$ is approximately a linear function of m. The approximation is better for the latter.
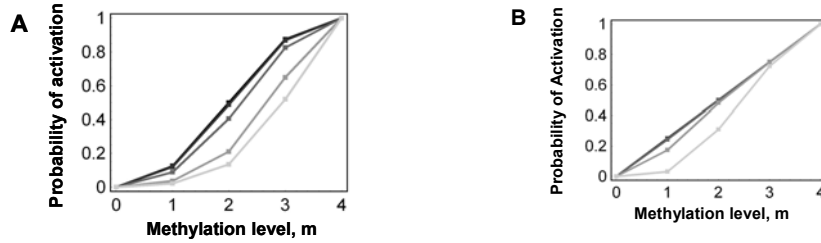

Figure S7: Probability of activation $a_m(L)$ of a Tar receptor complex as function of the methylation level of the receptor for increasing values of the external concentration of ligand: L = 0, 1, 10 and 100 μM aspartate (black to light grey). (**A**) Activation probabilities used in Figure 4 of the main text. We used similar values as in (17) for the dissociation constants (K_D = 1.7 μM and K_D^* = 12 μM) and for the probabilities of activation of a receptor complex free of attractant: p_0 = 0, p_1 = 0.125, p_2 = 0.5, p_3 = 0.874 and p_4 = 1.0. (**B**) Activation probabilities from Kollman et al. (20) based on measurements from Sourjik and Berg (16). For micromolar concentrations of ligand the probability of activation is approximately $a_m \cong m/4$. For (**B**) the approximation is excellent when L is in the micromolar range.

In previous models of bacterial chemotaxis (17, 19, 20), the probability of activation of receptors complexes at steady state increases approximately linearly with the number of methyl groups, $\bar{a}_m \approx m/m_{max}$, when the external concentration of ligand is small (Fig S7). Following these models we use $\beta = 1/m_{max}$ to plot our analytical solutions in Figs 2 and 3. In this case the adaptation term in Eq. 8 becomes exactly $\Delta A_{adapt}^* = \Delta M / m_{max}$. We validate our analytical results with stochastic simulations that include non-linear activation probabilities $a_m(L)$ (Figures S4C & S7). When considering the cooperative

interactions between receptors, $\beta = \bar{a}'(\bar{M})$ should be calculated by taking the derivative of the activation probability measured by Sourjik and Berg (16, 21, 22, 24-26, 28).

8. Large scale simulation of cells with CheB expressed at four times wild type level
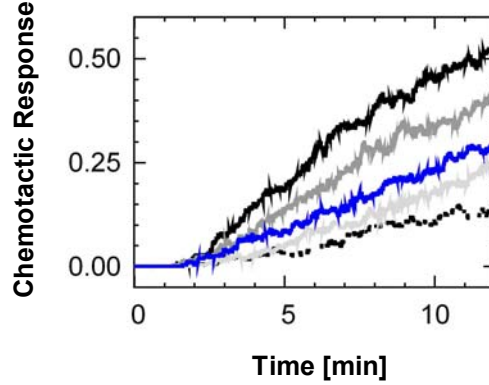
Figure S8: Effect of variations of [CheR] and [CheB] on the chemotactic response of a bacterial population of 400 cells. Digital swimming bacteria are exposed to a constant gradient of aspartate ($dL/dz = 10^{-8}$ M/μm, $L(z=0) = 1$ μM). Percentage of cells above $z = 1$ mm as a function of time: one (black), two (grey), four (light grey) wild-type [CheR] level. (Dashed line) response of wild type cells without gradient. (blue) Response of cells with wild-type level of [CheR] but four times the wild-type level of [CheB]. To ensure that this result is not due to [CheY-P] lying outside of the functioning range of the motor we adjusted the narrow functioning range of the motor so that the CW bias would remain the same in all populations expressing various level of [CheR] (CW bias=0.23).The initial position of the bacteria is $z = 0$ mm.

9. Appendix

Assuming quasi-equilibrium between the phosphorylated and unphosphorylated kinases, equation (S8) becomes

$$A_p \cong \left(1 + \frac{a_b B + a_y Y}{k_p A_{tot}^*}\right)^{-1} \cong \left(1 + \frac{a_y Y}{k_p A_{tot}^*}\right)^{-1} \tag{A1}$$

The second approximation is valid because $a_b B << a_y Y$. Linear perturbation of equation (A1) then gives:

$$\Delta A_p \cong \underbrace{\frac{a_y \overline{A}_p^2}{k_p \overline{A}_{tot}^*}}_{\theta_y} \Delta Y_p + \underbrace{\frac{(1 - A_p)A_p}{A_{tot}^*}}_{\theta_p} \Delta A_{tot}^* \tag{A2}$$

Using equation (A1) and (A2), the relaxation system (S23) reduces to

$$\frac{d}{dt}\begin{pmatrix} \Delta A^* \\ \Delta \varepsilon_{bp} \\ \Delta Y_p \end{pmatrix} \cong -\begin{pmatrix} \beta \tau_{GK}^{-1} & \beta g_b & 0 \\ -d_b \theta_b - a_b \overline{B}_b \theta_p (1 + \theta_b) & a_b \overline{A}_p + d_b (1 - \theta_c) - a_b \overline{B}_b \theta_p \theta_c & -a_b \overline{B} \theta_y \\ -a_y \overline{Y} \theta_p (1 + \theta_b) & -a_y \overline{Y} \theta_p \theta_c & a_y \overline{A}_p + d_y - a_y \overline{Y} \theta_y \end{pmatrix}\begin{pmatrix} \Delta A^* \\ \Delta \varepsilon_{bp} \\ \Delta Y_p \end{pmatrix} + \frac{d}{dt}\begin{pmatrix} \Delta A_{input}^* \\ 0 \\ 0 \end{pmatrix} \tag{A3}$$

Neglecting the small coupling of $\Delta \varepsilon_{bp}$ with ΔY_p (second row, third column of the matrix in A3) we find

$$\frac{d}{dt}\begin{pmatrix} \Delta A^* \\ \Delta \varepsilon_{bp} \end{pmatrix} \cong -\begin{pmatrix} \beta \tau_{GK}^{-1} & \beta g_b \\ -d_b \theta_b - a_b \overline{B}_b \theta_p (1 + \theta_b) & a_b \overline{A}_p + d_b (1 - \theta_c) - a_b \overline{B}_b \theta_p \theta_c \end{pmatrix}\begin{pmatrix} \Delta A^* \\ \Delta \varepsilon_{bp} \end{pmatrix} + \frac{d}{dt}\begin{pmatrix} \Delta A_{input}^* \\ 0 \end{pmatrix} \tag{A3}$$

Finally, assuming quasi-equilibrium for the phosphorylation-dephosphorylation of CheB (faster than methylation-demethylation) we obtain

$$\frac{\Delta \varepsilon_{bp}}{\overline{\varepsilon}_{bp}} \cong \underbrace{\frac{d_b \theta_b + a_b \overline{B}_b \theta_p (1 + \theta_b)}{a_b \overline{A}_p + d_b (1 - \theta_c) - a_b \overline{B}_b \theta_p \theta_c} \frac{\overline{A}^*}{\overline{\varepsilon}_{bp}}}_{\mu_a} \frac{\Delta A^*}{\overline{A}^*} \tag{A4}$$

10. References

1. Korobkova, E., Emonet, T., Vilar, J. M. G., Shimizu, T. S., & Cluzel, P. (2004) *Nature* **428,** 574-578.
2. Spudich, J. L. & Koshland, D. E. (1976) *Nature* **262,** 467-471.
3. Rosenfeld, N., Young, J. W., Alon, U., Swain, P. S., & Elowitz, M. B. (2005) *Science* **307,** 1962-1965.
4. Elowitz, M. B., Levine, A. J., Siggia, E. D., & Swain, P. S. (2002) *Science* **297,** 1183-1186.
5. Golding, I., Paulsson, J., Zawilski, S. M., & Cox, E. C. (2005) *Cell* **123,** 1025-1036.
6. Le, T. T., Harlepp, S., Guet, C. C., Dittmar, K., Emonet, T., Pan, T., & Cluzel, P. (2005) *Proc Natl Acad Sci U S A*.
7. Raser, J. M. & O'Shea, E. K. (2004) *Science* **304,** 1811-1814.
8. Pedraza, J. M. & van Oudenaarden, A. (2005) *Science* **307,** 1965-1969.

9.   Swain, P. S., Elowitz, M. B., & Siggia, E. D. (2002) *Proc Natl Acad Sci U S A* **99,** 12795-12800.
10.   Paulsson, J. (2004) *Nature* **427,** 415-418.
11.   Kubo, R. (1957) *Journal of the Physical Society of Japan* **12,** 570-586.
12.   Callen, H. B. & Greene, R. F. (1952) *Phys Rev* **86,** 702-710.
13.   Onsager, L. & Machlup, S. (1953) *Phys Rev* **91,** 1505-1512.
14.   Asakura, S. & Honda, H. (1984) *J Mol Biol* **176,** 349-367.
15.   Barkai, N. & Leibler, S. (1997) *Nature* **387,** 913-917.
16.   Sourjik, V. & Berg, H. C. (2002) *Proc Natl Acad Sci U S A* **99,** 123-127.
17.   Morton-Firth, C. J., Shimizu, T. S., & Bray, D. (1999) *J Mol Biol* **286,** 1059-1074.
18.   Mello, B. A. & Tu, Y. (2003) *Biophysical Journal* **84,** 2943-2956.
19.   Rao, C. V., Kirby, J. R., & Arkin, A. P. (2004) *PLoS Biol* **2,** E49.
20.   Kollmann, M., Lovdok, L., Bartholome, K., Timmer, J., & Sourjik, V. (2005) *Nature* **438,** 504-507.
21.   Shimizu, T. S., Aksenov, S. V., & Bray, D. (2003) *J Mol Biol* **329,** 291-309.
22.   Duke, T. A. J. & Bray, D. (1999) *P Natl Acad Sci USA* **96,** 10104-10108.
23.   Mello, B. A. & Tu, Y. H. (2003) *P Natl Acad Sci USA* **100,** 8223-8228.
24.   Sourjik, V. & Berg, H. C. (2004) *Nature* **428,** 437-441.
25.   Keymer, J. E., Endres, R. G., Skoge, M., Meir, Y., & Wingreen, N. S. (2006) *Proc Natl Acad Sci U S A*.
26.   Mello, B. A. & Tu, Y. (2005) *Proc Natl Acad Sci U S A* **102,** 17354-17359.
27.   Rao, C. V., Frenklach, M., & Arkin, A. P. (2004) *J Mol Biol* **343,** 291-303.
28.   Endres, R. G. & Wingreen, N. S. (2006) *Proc Natl Acad Sci U S A* **103,** 13040-13044.
29.   Sourjik, V. & Berg, H. C. (2002) *Proceedings of the National Academy of Sciences of the United States of America* **99,** 12669-12674.
30.   Goldbeter, A. & Koshland, D. E. (1981) *Proceedings of the National Academy of Sciences of the United States of America-Biological Sciences* **78,** 6840-6844.
31.   Borkovich, K. A., Alex, L. A., & Simon, M. I. (1992) *Proc Natl Acad Sci U S A* **89,** 6756-6760.
32.   Yi, T. M., Huang, Y., Simon, M. I., & Doyle, J. (2000) *P Natl Acad Sci USA* **97,** 4649-4653.
33.   Berg, O. G., Paulsson, J., & Ehrenberg, M. (2000) *Biophysical Journal* **79,** 1228-1236.
34.   Elf, J., Paulsson, J., Berg, O. G., & Ehrenberg, M. (2003) *Biophysical Journal* **84,** 154-170.
35.   Detwiler, P. B., Ramanathan, S., Sengupta, A., & Shraiman, B. I. (2000) *Biophys J* **79,** 2801-2817.
36.   Kampen, N. G. v. (1992) *Stochastic processes in physics and chemistry* (North-Holland, Amsterdam ; New York).
37.   Chen, Y.-D. (1978) *Adv. Chemical Physics* **37,** 67-97.
38.   Elf, J. & Ehrenberg, M. (2003) *Genome Research* **13,** 2475-2484.
39.   Gardiner, C. W. (1985) *Handbook of stochastic methods for physics, chemistry, and the natural sciences* (Springer-Verlag, Berlin ; New York).
40.   Koshland, D. E., Jr. (1998) *Science* **280,** 852-853.
41.   Shibata, T. & Fujimoto, K. (2005) *Proc Natl Acad Sci U S A* **102,** 331-336.

42. Chock, P. B. & Stadtman, E. R. (1977) *P Natl Acad Sci USA* **74,** 2766-2770.
43. Ferrell, J. E., Jr. & Machleder, E. M. (1998) *Science* **280,** 895-898.
44. Melen, G., Levy, S., Barkai, N., & Shilo, B. (2005) *Mol Syst Biol***,** doi:10.1038/msb4100036.
45. Li, M. S. & Hazelbauer, G. L. (2004) *Journal of Bacteriology* **186,** 3687-3694.
46. Simms, S. A., Stock, A. M., & Stock, J. B. (1987) *Journal of Biological Chemistry* **262,** 8537-8543.
47. Barnakov, A. N., Barnakova, L. A., & Hazelbauer, G. L. (2002) *Journal of Biological Chemistry* **277,** 42151-42156.
48. Shrout, A. L., Montefusco, D. J., & Weis, R. M. (2003) *Biochemistry* **42,** 13379-13385.
49. Stewart, R. C., Jahreis, K., & Parkinson, J. S. (2000) *Biochemistry* **39,** 13157-13165.
50. Levin, M. D. & Bray, D. (2006).
51. Rao, C. V. & Arkin, A. P. (2003) *Journal of Chemical Physics* **118,** 4999-5010.
52. Wu, J., Li, J., Li, G., Long, D. G., & Weis, R. M. (1996) *Biochemistry* **35,** 4984-4993.
53. Chalah, A. & Weis, R. M. (2005) *Bmc Microbiology* **5**.
54. Antommattei, F. M., Munzner, J. B., & Weis, R. M. (2005) *Journal of Bacteriology* **187,** 811-811.
55. Lai, W. C. & Hazelbauer, G. L. (2005) *J Bacteriol* **187,** 5115-5121.
56. Perez, E., West, A. H., Stock, A. M., & Djordjevic, S. (2004) *Biochemistry* **43,** 953-961.
57. Li, M. & Hazelbauer, G. L. (2005) *Molecular microbiology* **56,** 1617-1626.
58. Boldog, T., Grimme, S., Li, M., Sligar, S. G., & Hazelbauer, G. L. (2006) *Proc Natl Acad Sci U S A* **103,** 11509-11514.
59. Andrews, B. W., Yi, T. M., & Iglesias, P. A. (2006) *PLoS computational biology* **2,** e154.
60. Alon, U., Surette, M. G., Barkai, N., & Leibler, S. (1999) *Nature* **397,** 168-171.
61. Terwilliger, T. C., Wang, J. Y., & Koshland, D. E., Jr. (1986) *Proc Natl Acad Sci U S A* **83,** 6707-6710.